INTERNATIONAL JOURNAL OF PRECISION ENGINEERING AND MANUFACTURING Vol. 16, No. 13, pp. 2699-2707 DECEMBER 2015 / 2699
DOI: 10.1007/s12541-015-0345-1 ISSN 2234-7593 (Print) / ISSN 2005-4602 (Online)

# Correction Functions to Determine the Stress State of a Flattened Disk Specimen in Diametral Testing with Reference to Analytical Solutions for Circular Specimens

**Hyunho Shin[1,#] and Jong-Bong Kim[2,#]**

1 Mechanics of Materials Laboratory, Department of Materials Engineering, Gangneung-Wonju National University, 7 Jukheon-gil, Gangneung-si, Gangwon-do, 25457, South Korea
2 Computational Mechanics and Design Laboratory, Department of Mechanical and Automotive Engineering, Seoul National University of Science and Technology, 232 Gongneung-ro, Nowon-gu, Seoul, 01811, South Korea
# Corresponding Author / E-mail: hshin@gwnu.ac.kr, TEL: +82-33-640-2484, FAX: +82-33-640-2244
E-mail: jbkim@seoultech.ac.kr, TEL: +82-2-970-6434, FAX: +82-2-979-7032

KEYWORDS: Diametral test, Flattened disk specimen, Circular specimen, Correction function

*The correction functions that can be used to determine the stress state of a flattened disk specimen in diametral testing are provided by referring to the analytical solutions for arc- and point-loaded circular specimens. The stress components at three important locations in the flattened specimen (with varying degrees of truncation, w) were obtained numerically by finite element analysis, and compared with the analytical solutions at the center of the arc- and point-loaded specimens. The correction functions, which are provided as a function of w, can be useful tools for the analysis of the stress state and for the design of the flattened disk specimen in diametral testing.*

Manuscript received: June 28, 2015 / Revised: September 1, 2015 / Accepted: September 9, 2015

## 1. Introduction

The diametral test, which is called by many names, such as Brazilian test, indirect tensile test, and splitting test, was originally developed to determine the tensile strength of concretes[1,2] in the early 1950s using a 2D analytical solution (Hertz solution[3,4]). Over the last few decades, it was increasingly used to measure the strength of various materials, including ceramics, rocks, alloys, cements, glasses, coals, polymers, pharmaceuticals, powder compacts, and asphalts.[5-7]

For specimens homogeneous in macroscopic scale (e.g., concretes), a 3D cylinder specimen with a notable thickness needs to be tested; a 3D solution is needed to accurately determine the tensile strength of those specimens. Brittle specimens[8-12] made of ceramics and glasses (also some rocks) are homogeneous in microscopic scale. In such cases, the disk-type specimen with the thickness to diameter ratio of less than approximately 0.2 can be used by referring to the 2D Hertz solution.

In the diametral test, a circular cylindrical disk specimen is subjected to a compressive load through two diametrally opposite rigid platens. Thus far, two types of loading platens were used for loading the diametral specimen: a flat platen (Fig. 1) and a platen with a concave circular shape (Fig. 2). The specimen loaded by the flat platen (Fig. 1(a)) is usually analyzed by the Hertz solution which considers a point loading (Fig. 1(b)). As we describe in the next section, along the loading axis ($y$-axis), $\sigma_x$ is positive (tensile) and does not vary with position (Hertz solution[3,4]). The tensile strength of the diametral specimen is determined under the assumption that the Hertz solution is valid: the point-loaded specimen fails by the developed tensile stress ($\sigma_x$) along the loading axis.

In the conventional diametral test with such point loading, there is also a compressive stress ($\sigma_y$) that varies from three times the magnitude of the tensile stress ($\sigma_x$) at $y$=0 to infinity at $y$=$R$. Because of the excessively high magnitude of the compressive stress ($\sigma_y$), the failure of the specimen may be initiated by the compressive stress at the point-loading region rather than by the tensile stress in the loading axis. Then, the load is *distributed* over a finite area due to the failure of the loading region; the required assumption for the Hertz solution (point loading) is violated and thus the reliability of the measured tensile strength is lowered.

The specimen loaded by the platen with a concave circular shape (Fig 2(a)) may be analyzed suitably by the Hondros solution[13] (Fig. 2(b)). Although the platen delivers the load over a finite arc area of the specimen, the specimen is loaded in the *vertical* ($y$) direction (Fig.

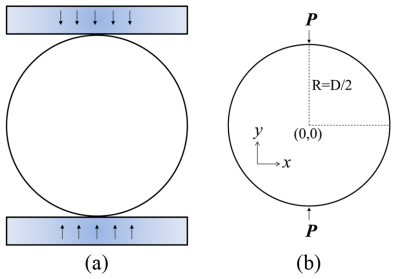


Fig. 1 (a) Circular specimen loaded by a flat platen and (b) the geometry considered in the Hertz solution. $P$ is the applied load

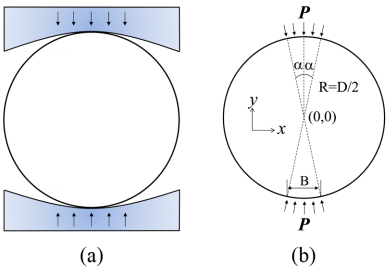


Fig. 2 (a) Circular specimen loaded by a concave-shaped circular platen and (b) the geometry considered in the Hondros solution. $P$ is the applied load

2(a)). The Hondros solution, however, considers loading *toward the center* of the specimen (Fig. 2(b)). When the arc length is small (the B/D value of less than approximately 0.05), the Hondros solution may be a reasonable approximation to the real case of vertical loading because the load delivered through the concave-shaped platen over a small arc length is aligned practically in the vertical direction. When the arc length is small, however, as will be seen later, the development of the excessively high magnitude of the compressive stress ($\sigma_y$) in the loading region is inevitable like the case of the point loading that uses a flat platen.

As mentioned, pre-failure of the specimen may initiate in the loading region by the development of the excessively high magnitude of the compressive stress ($\sigma_y$). Such pre-failure alters the stress state in the diametral specimen, resulting in an unreliable test result. Compared with the static diametral test, the necessity of avoiding the stress-concentration-induced pre-failure is much higher in a dynamic diametral test, which is usually carried out using the split Hopkinson bar (SHB). In the SHB test of the diametral specimen,[14-27] a disk specimen is point- or arc-loaded by the end surfaces of two long bars (the input bar and output bar). The stress wave enters and transmits the specimen through the two loading regions. If the stress-concentration-induced pre-failure occurs in the loading regions, the entrance and transmittance of the stress wave through the contact regions are perturbed. Then, the signals of the stress wave representing the dynamic tensile strength of the specimen is distorted, resulting in an unreliable test result. Therefore, the phenomenon of stress wave distortion due to the pre-failure highly necessitates a way to avoid the stress-concentration in the loading region of the SHB.

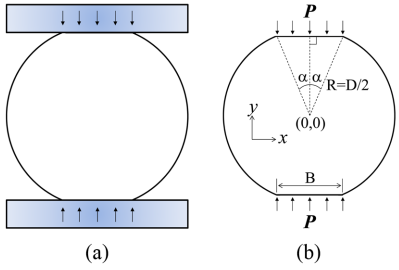


Fig. 3 (a) Flattened specimen loaded by a flat platen and (b) the geometry corresponding to the Hondros solution. $P$ is the applied load

From the perspective of avoiding such a stress-concentration-induced pre-failure in the loading region, this study focuses on a flattened disk specimen,[25-29] as illustrated in Fig. 3. As will be seen later in this study, use of the flattened specimen greatly reduces the concentration of the compressive stress ($\sigma_y$) in the loading region. Another important aspect of using the flattened specimen is that vertical loading to the flattened specimen is achieved very suitably in the experiment using a flat platen (Fig. 3(a)). However, there is no available analytical solution to determine the stress state of a flattened specimen, which is the reason here we aimed to obtain a way to determine the stress state in the *flattened* specimen with references to the available analytical solutions for a *circular* specimen. Once the way to describe the stress state of the flattened disk specimen is available, the flattened *disk* specimen will be useful for determining the tensile strength of brittle materials that are homogeneous in microscopic scale. The flattened disk specimen will be useful not only in the static test but also, as mentioned, in the dynamic tensile test using the SHB instrument.

Once we obtain the stress state of the flattened disk specimen numerically, the ratio of the numerical solution to a given analytical solution can be obtained. Here we report the correction functions with references to the analytical solutions for the arc-loaded circular disk specimen (Hondros solution) and the point-loaded circular disk specimen (Hertz solution).

## 2. Analytical Solutions and the Correction Functions

### 2.1 Hertz solution

In order to determine the tensile strength of the disk specimen loaded by the flat platen (Fig. 1(a)), as mentioned, the Hertz solution is usually used. The Hertz solution (under a 2D plane stress condition)[4] was summarized by Frocht[3] as follows. On the $x$-axis (Fig. 1(b)), the Hertz solution is

$$\sigma_x = \frac{2P}{\pi t D}\left[\frac{D^2-4x^2}{D^2+4x^2}\right]^2 \tag{1}$$

$$\sigma_y = -\frac{2P}{\pi t D}\left[\frac{4D^2}{(D^2+4x^2)^2}-1\right] \tag{2}$$

$$\tau_{xy} = 0 \tag{3}$$

where $D$ and $t$ are the diameter and thickness of the specimen,

respectively, and $P$ is the applied load. On the $y$-axis,

$$\sigma_x = \sigma_{x,center}^{point} = 2P/\pi tD \tag{4}$$

$$\sigma_y = -\frac{2P}{\pi tD}\left[\frac{2D}{D-2y}+\frac{2D}{D+2y}-1\right] \tag{5}$$

$$\tau_{xy} = 0 \tag{6}$$

At the center ($x = y = 0$) of the point-loaded specimen, $\sigma_x$ is given by Eq. (4) and $\sigma_y$ is

$$\sigma_{y,center}^{point} = -6P/\pi tD \tag{7}$$

Thus, along the loading axis ($y$-axis), $\sigma_x$ is positive (tensile) and does not vary with position (Eq. (4)). According to Eq. (7), at the center of the specimen, $\sigma_y$ is compressive and is three times the magnitude of $\sigma_x$ at the center (Eq. (4)). The magnitude of $\sigma_y$ increases along the loading axis to infinity at the end of the specimen ($y = D/2$; See Eq. (5)). If a brittle specimen, which is usually weak in tension, fails solely by tension developed in the loading axis, Eq. (4) (and Eq. (1) at $x$=0) can be used to determine the tensile strength of the specimen ($\sigma_f$):

$$\sigma_f^{point} = 2P_f/\pi tD \tag{8}$$

where $P_f$ is the load at the failure of the specimen.

### 2.2 Hondros solution

In 1959, Hondros[13] developed 2D analytical solutions for the case when the load is applied over the two diametrically opposite arcs of angular width $2\alpha$ (Fig. 2(b)). His solutions are as follows. Along the $x$-axis,

$$\sigma_x = \frac{2P}{\pi tD\alpha}\left[\frac{(1-x^2/R^2)\sin 2\alpha}{1+2(x^2/R^2)\cos 2\alpha + x^4/R^4} - \tan^{-1}\left(\frac{1-x^2/R^2}{1+x^2/R^2}\tan\alpha\right)\right] \tag{9}$$

$$\sigma_y = -\frac{2P}{\pi tD\alpha}\left[\frac{(1-x^2/R^2)\sin 2\alpha}{1+2(x^2/R^2)\cos 2\alpha + x^4/R^4} + \tan^{-1}\left(\frac{1-x^2/R^2}{1+x^2/R^2}\tan\alpha\right)\right] \tag{10}$$

$$\tau_{xy} = 0 \tag{11}$$

where $R = D/2$. Along the $y$-axis,

$$\sigma_x = \frac{2P}{\pi tD\alpha}\left[\frac{(1-y^2/R^2)\sin 2\alpha}{1+2(y^2/R^2)\cos 2\alpha + y^4/R^4} - \tan^{-1}\left(\frac{1-y^2/R^2}{1+y^2/R^2}\tan\alpha\right)\right] \tag{12}$$

$$\sigma_y = -\frac{2P}{\pi tD\alpha}\left[\frac{(1-y^2/R^2)\sin 2\alpha}{1+2(y^2/R^2)\cos 2\alpha + y^4/R^4} + \tan^{-1}\left(\frac{1-y^2/R^2}{1+y^2/R^2}\tan\alpha\right)\right] \tag{13}$$

$$\tau_{xy} = 0 \tag{14}$$

At the center of the arc-loaded specimen ($x = y = 0$), $\sigma_x$ (Eqs. (9) and (12)) becomes

$$\sigma_{x,center}^{arc} = \frac{2P}{\pi tD\alpha}[\sin 2\alpha - \alpha] \tag{15}$$

and $\sigma_y$ (Eqs. (10) and (13)) becomes

$$\sigma_{y,center}^{arc} = -\frac{2P}{\pi tD\alpha}[\sin 2\alpha + \alpha] \tag{16}$$

When $\alpha$ is small, $\sin 2\alpha \fallingdotseq 2\alpha$, and thus Eqs. (15) and (16) become Eqs. (4) and (7), respectively, which are the Hertz solutions at the center of the point-loaded specimen. If the arc-loaded specimen fails solely by tension developed in the loading axis, Eq. (15) can be used to determine the tensile strength of the arc-loaded specimen ($\sigma_f^{arc}$):

$$\sigma_f^{arc} = \frac{2P_f}{\pi tD\alpha}[\sin 2\alpha - \alpha] \tag{17}$$

### 2.3 Correction functions

For the *flattened* specimen (Fig. 3), note that the normalized flattened length with respect to the diameter, B/D, is related to $\alpha$:

$$B/D = \sin\alpha \tag{18}$$

Eq. (18) means that, for a given B/D value of the flattened specimen, there is a correspondent $\alpha$ value of the arc-loaded specimen. (In this study, the term B/D is preferentially used instead of $\alpha$ as this study focuses on the flattened specimen.) Because of the correlation between B/D and $\alpha$, it is worthwhile to investigate how much difference exists between the stress state of the flattened specimen with a given B/D and that of the arc-loaded specimen with the corresponding $\alpha$ value.

Since, as mentioned, there is no analytical solution for the normally loaded flattened specimen, this study first numerically determines the stress state of the flattened specimen based on finite element analysis. Then, for a given stress component ($\sigma_x$ or $\sigma_y$), the stress ratio of the flattened specimen to the arc-loaded specimen, that is the correction function, is obtained. The stress ratio of the flattened specimen to the point-loaded specimen is also obtained. The correction functions (named $E$ and $e$) for $\sigma_x$ at the center of the flattened specimen are

$$E(B/D) \equiv \sigma_{x,center}^{flattened}/\sigma_{x,center}^{arc} \tag{19}$$

$$e(B/D) \equiv \sigma_{x,center}^{flattened}/\sigma_{x,center}^{point} \tag{20}$$

where $\sigma_{x,center}^{flattened}$ is the numerical solution for a given B/D value at the center of the flattened specimen, $\sigma_{x,center}^{arc}$ is the Hondros solution (Eq. (15)) for the arc-loaded specimen with an $\alpha$ value corresponding to the B/D value of the flattened specimen, and $\sigma_{x,center}^{point}$ is the Hertz solution (Eq. (4)) for the point-loaded specimen without regard to the B/D value of the flattened specimen. In Eqs. (19) and (20), the same load $P$ is considered for both the numerator and denominator in each equation.

This study also provides the correction functions for $\sigma_y$ at the center of the flattened specimen:

$$F(B/D) \equiv \sigma_{y,center}^{flattened}/\sigma_{y,center}^{arc} \tag{21}$$

$$f(B/D) \equiv \sigma_{y,center}^{flattened}/\sigma_{y,center}^{point} \tag{22}$$

where the meanings of the terms for $\sigma_y$ are the same as those for $\sigma_x$ in Eqs. (19) and (20).

In order to obtain stress information at the end (loading portion) of the flattened specimen, the correction functions for $\sigma_x$ and $\sigma_y$ are defined as

$$G(B/D) \equiv \sigma_{x,end}^{flattened}/\sigma_{x,center}^{arc} \tag{23}$$

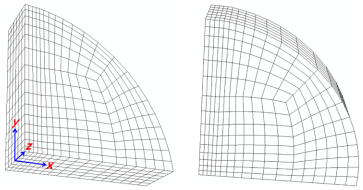

(a) (b)

Fig. 4 Finite element model when B/D = 0.1. (a) The model with the axes and (b) a different view of the model showing the top-flattened area

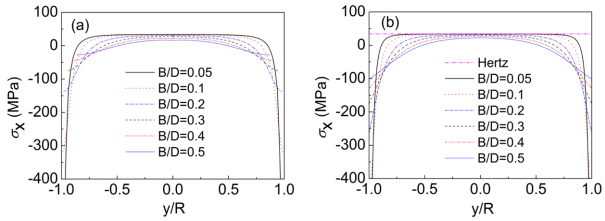


Fig. 5 $\sigma_x$ along the $y$-axis: (a) The numerical solutions for the flattened specimen with varying B/D values and (b) the Hondros solutions for the arc-loaded specimen with corresponding $\alpha$ values

$$g(B/D) \equiv \sigma_{x,end}^{flattened} / \sigma_{x,center}^{point} \tag{24}$$

$$H(B/D) \equiv \sigma_{y,end}^{flattened} / \sigma_{y,center}^{arc} \tag{25}$$

$$h(B/D) \equiv \sigma_{y,end}^{flattened} / \sigma_{y,center}^{point} \tag{26}$$

where $\sigma_{x,end}^{flattened}$ and $\sigma_{y,end}^{flattened}$ are the numerical solutions at the end (loading portion) of the flattened specimen with a given B/D value and the denominators in each equation are the analytical solutions defined in Eqs. (19)-(22).

As we show later in section 4, the magnitude of $\sigma_y$ in the loading axis of the flattened specimen is not maximum at the end (loading portion) of the specimen but the maximum magnitude appears at some distance away from the end of the specimen in the loading axis. This study provides the correction functions that are used to determine stresses at such a location ( $\sigma_{x,max}^{flattened}$ and $\sigma_{y,max}^{flattened}$ ) with references to the analytical solutions:

$$J(B/D) \equiv \sigma_{x,max}^{flattened} / \sigma_{x,center}^{arc} \tag{27}$$

$$j(B/D) \equiv \sigma_{x,max}^{flattened} / \sigma_{x,center}^{point} \tag{28}$$

$$K(B/D) \equiv \sigma_{y,max}^{flattened} / \sigma_{y,center}^{arc} \tag{29}$$

$$k(B/D) \equiv \sigma_{y,max}^{flattened} / \sigma_{y,center}^{point} \tag{30}$$

## 3. Numerical Analysis

The diameter of the considered specimen was 100 mm. In order to ensure the plane stress condition, the thickness ($t$) of the specimen was sufficiently thin (15 mm); the $t/D$ ratio was 0.15. The considered B/D ratios of the flattened specimen were 0.05, 0.1, 0.2, 0.3, 0.4, and 0.5, which correspond to the $\alpha$ values (in radian) of 0.050, 0.100, 0.201, 0.305, 0.412, and 0.524. Considering the symmetry of the flattened specimen in the diametral test, one quarter space of the specimen was discretized using eight node linear brick elements as seen in Fig. 4. The size of the meshes passed a separate mesh quality test. The nodes at $z$-$x$ and $y$-$z$ planes were not allowed to move along the $y$ and $x$ directions, respectively, to account for symmetry. A 40 kN load was applied on the top flattened surface of the quarter model using an analytically rigid surface. The elastic modulus and Poisson's ratio of the specimen were 310 GPa and 0.31, respectively, which are comparable to the SiC ceramic material. A commercial finite element package Abaqus was used for the numerical analysis. After the numerical calculation by the finite element method, the values of $\sigma_x$ and $\sigma_y$ were extracted along the line paths of the $x$- and $y$-axes, from which the correction functions were determined.

## 4. Results and Discussion

### 4.1 $\sigma_x$ profiles

The profiles of the tensile stress ($\sigma_x$) in the flattened specimen (the numerical solution) are shown in Fig. 5(a) along the loading axis ($y$-axis) for varying B/D values.[1] The stress profiles (the Hondros solution) in the arc-loaded specimen with $\alpha$ values corresponding to the B/D value of the flattened specimen are shown in Fig. 5(b). Included in Fig. 5(b) is the Hertz solution for the point-loaded specimen. It is the same as the Hondros solution when $\alpha = 0$.

Along the $y$-axis for both specimens, (1) the tensile stress ($\sigma_x$) is maximal at the center of the specimen. (2) The maximum tensile stress at the center decreases as the B/D value increases. (3) As the position moves toward the loading point ($y$/R=1), $\sigma_x$ becomes compressive and (4) this compressive stress appears earlier as the B/D value increases. On a quantitative basis, the maximum tensile stress at the center of the flattened specimen for a given B/D value is slightly lower than that of the corresponding arc-loaded specimen.

The profiles of the tensile stress ($\sigma_x$) in the flattened specimen are now shown along the $x$-axis in Fig. 6(a) for varying B/D values. The Hondros solutions for the arc-loaded specimen are shown in Fig. 6(b). The profiles of the tensile stress ($\sigma_x$) along the $x$-axis are also qualitatively similar for both specimens; it is maximal at the center of the specimen and the maximum magnitude decreases with the B/D value.

### 4.2 $\sigma_y$ profiles

The profiles of $\sigma_y$ in the flattened specimen are shown in Fig. 7(a) along the loading axis ($y$-axis) for varying B/D values. The Hondros

1. After the numerical solution was obtained from the quarter space of the specimen in the ranges of $0 \le x \le R$ and $0 \le y \le R$, the numerical results in the ranges of $-R \le x \le 0$ and $-R \le y \le 0$ were constructed considering the symmetry of the specimen throughout this study.

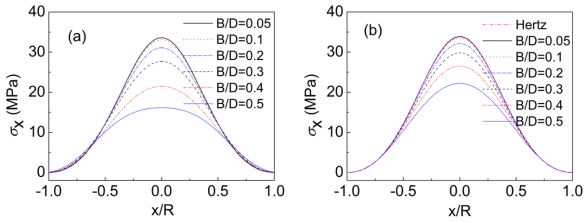


Fig. 6 $\sigma_x$ along the $x$-axis: (a) The numerical solutions for the flattened specimen with varying B/D values and (b) the Hondros solutions for the arc-loaded specimen with corresponding $\alpha$ values

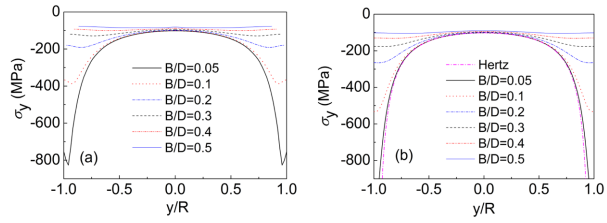


Fig. 7 $\sigma_y$ along the $y$-axis: (a) The numerical solutions for the flattened specimen with varying B/D values and (b) the Hondros solutions for the arc-loaded specimen with corresponding $\alpha$ values

solutions for the arc-loaded specimen are shown in Fig. 7(b). Along the $y$-axis, for both specimens, as the B/D value increases, the magnitude of the compressive stress ($\sigma_y$) at the loading portion of the specimen decreases significantly. This is certainly a benefit of the arc-loaded and the flattened specimens in that the failure of the specimens at the loading portion by the excessively developed compressive stress can be avoided if an appropriate B/D value is selected. The selection of an overly high value of the B/D value sacrifices the development of the important tensile stress ($\sigma_x$) at the center of the specimen (see Figs. 5 and 6), which causes the tensile fracture of the specimen; thus, an appropriate B/D value needs to be selected with this point in mind.

As seen in Fig. 7(a), in the loading axis of the flattened specimen, the magnitude of $\sigma_y$ is not maximum at the end (loading portion) of the specimen but the maximum magnitude appears at some distance away from the end (loading portion) of the specimen. This interesting phenomenon is similar to the phenomenon that appears when a material is indented by an indenter:[30,31] the maximum pressure does not appear at the interface between the indenter and specimen but it develops at some distance beneath the indenter/specimen interface.

The profiles of $\sigma_y$ in the flattened specimen are now shown along the $x$-axis in Fig. 8(a) for varying B/D values. The Hondros solutions for the arc-loaded specimen are shown in Fig. 8(b) along the same $x$-axis. The profiles of the compressive stress ($\sigma_y$) are also qualitatively similar for both specimens. The compressive stress along the $x$-axis is also maximal at the center of the specimen like $\sigma_x$ (See Fig. 6), and the maximum magnitude decreases with B/D.

### 4.3 Correction functions at the center

Assuming that the failure of the specimen takes place at the center of the specimen solely by the developed tensile stress, if the correction functions $E$(B/D) (the ratio of $\sigma_{x,center}^{flattened}/\sigma_{x,center}^{point}$) and $e$(B/D) (the ratio of $\sigma_{x,center}^{flattened}/\sigma_{x,center}^{point}$) are known, the fracture strength of the flattened specimen ($\sigma_f^{flattened}$) with an arbitrary B/D value can be determined with references to the analytical solutions. To obtain correction functions $E$(B/D) and $e$(B/D), $\sigma_{x,center}^{flattened}$ were taken from Fig. 5(a) (or Fig. 6(a)) for varying B/D values and $\sigma_{x,center}^{arc}$ was taken from Fig. 5(b) (or Fig. 6(b)) for varying $a$ values corresponding to the B/D values of the flattened specimen. The constructed values of $E$(B/D) and $e$(B/D) are shown in Fig. 9(a).[2] The solid curves in Fig. 9(a) result from polynomial fitting of the data points using

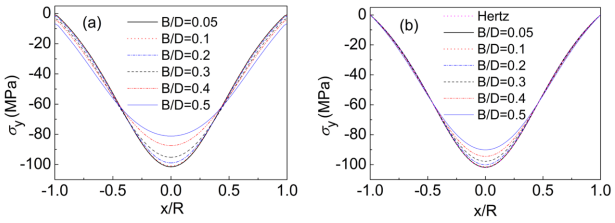


Fig. 8 $\sigma_y$ along the x-axis: (a) The numerical solutions for the flattened specimen with varying B/D values and (b) the Hondros solutions for the arc-loaded specimen with corresponding $\alpha$ values

$$L(w) = A_0 + A_1 w + A_2 w^2 + A_3 w^3 \tag{31}$$

where $L$ is the fitting function (for the correction functions $E$, $e$, $F$, and $f$), $w$ is B/D, and $A_0$, $A_1$, $A_2$, and $A_3$ are the fitting parameters shown in Table 1.

As seen in Fig. 9, the correction functions decrease gradually up to the B/D value of 0.3 while they decrease rather abruptly thereafter. Therefore, to provide accurate fitting parameters, we fitted the data points separately for the $w$ (=B/D) range of $0 \le w \le 0.3$ and $0.3 \le w \le 0.5$, as seen in Table 1. In separate trials (not shown), data fitting over the whole available B/D range was not as successful as predicting the data points in two separate B/D ranges.

Using correction functions $E$(B/D) and $e$(B/D), the fracture strength of the flattened specimen ($\sigma_f^{flattened}$) with an arbitrary B/D value can be determined:

$$\sigma_f^{flattened} = E(B/D)\sigma_f^{arc} = E(B/D)\frac{2P_f}{\pi tD\alpha}[\sin 2\alpha - \alpha] \tag{32}$$

$$\sigma_f^{flattened} = e(B/D)\sigma_f^{point} = e(B/D)\frac{2P_f}{\pi tD} \tag{33}$$

where $P_f$ is the load at the moment of the fracture of the flattened specimen; Eq. (17) was plugged into Eq. (32) for $\sigma_f^{arc}$ and Eq. (8) was plugged into Eq. (33) for $\sigma_f^{point}$.

The ratios of $\sigma_{y,center}^{flattened}/\sigma_{y,center}^{arc}$ (for $F$(B/D)) and $\sigma_{y,center}^{flattened}/\sigma_{y,center}^{point}$ (for $f$(B/D)) were obtained using the data shown in Fig. 7 (or Fig. 8). The determined values of $F$(B/D) and $f$(B/D) are shown in Fig. 9(b).

2. The theoretical value (unity) of the correction functions at B/D=0 were added in this study because the validity of the finite element solution for this case compared with the analytical solutions is well documented.[28,29]

Table 1 Parameters for the fitting function $L$ (Eq. (31))

| Correction functions | Range of $w$ (=B/D) | $A_0$ | $A_1$ | $A_2$ | $A_3$ | $R^2$ |
|---|---|---|---|---|---|---|
| $E$ | $0 \le w \le 0.3$ | 1 | -0.12926 | 0.26056 | -2.04707 | 1.00000 |
| | $0.3 \le w \le 0.5$ | 1.51085 | -2.49594 | 1.85980 | 0 | NA |
| $e$ | $0 \le w \le 0.3$ | 1 | -0.12472 | -1.15916 | -1.54791 | 1.00000 |
| | $0.3 \le w \le 0.5$ | 1.52260 | -2.74419 | 1.30194 | 0 | NA |
| $F$ | $0 \le w \le 0.3$ | 1 | -0.04529 | 0.10978 | 0.06694 | 1.00000 |
| | $0.3 \le w \le 0.5$ | 1.25497 | -1.27649 | 1.13514 | 0 | NA |
| $f$ | $0 \le w \le 0.3$ | 1 | -0.04487 | -0.34223 | -0.77891 | 1.00000 |
| | $0.3 \le w \le 0.5$ | 1.24781 | -1.25554 | 0.70642 | 0 | NA |

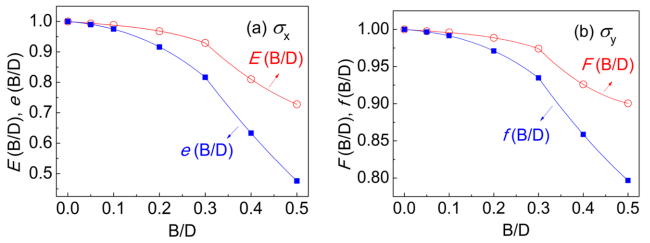


Fig. 9 Correction functions to determine (a) $\sigma_x$ and (b) $\sigma_y$ at the center of the flattened specimen

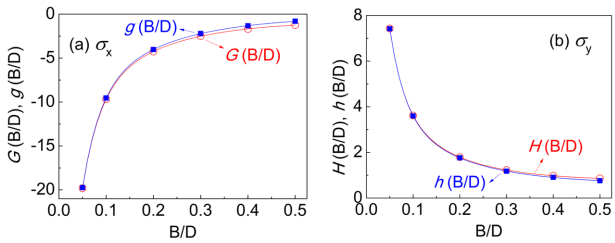


Fig. 10 Correction functions to determine (a) $\sigma_x$ and (b) $\sigma_y$ at the end (loading portion) of the flattened specimen

The solid curves in Fig. 9(b) result from polynomial fitting of the $F$(B/D) and $f$(B/D) values using Eq. (31) and the fitting constants are shown in Table 1. At a given load $P$, the functions $F$(B/D) and $f$(B/D) allow the determination of the compressive stress ($\sigma_y$) of the flattened specimen with references to the Hondros solution and Hertz solution, respectively:

$$\sigma_{y,center}^{flattened} = F(B/D)\sigma_{y,center}^{arc} = -F(B/D)\frac{2P}{\pi tD\alpha}[\sin 2\alpha + \alpha] \quad (34)$$

$$\sigma_{y,center}^{flattened} = f(B/D)\sigma_{y,center}^{point} = -f(B/D)\frac{6P}{\pi tD} \quad (35)$$

### 4.4 Correction functions at the loading portion

In order to obtain the correction functions used to determine $\sigma_x$ at the end (loading portion) of the flattened specimen, the ratios of $\sigma_{x,end}^{flattened}/\sigma_{x,center}^{arc}$ (for $G$(B/D)) and $\sigma_{x,end}^{flattened}/\sigma_{x,center}^{point}$ (for $g$(B/D)) were obtained from the data shown in Fig. 5. For the correction functions $H$(B/D) and $h$(B/D), which are used to determine $\sigma_y$, the ratios of $\sigma_{y,end}^{flattened}/\sigma_{y,center}^{arc}$ (for $H$(B/D)) and $\sigma_{y,end}^{flattened}/\sigma_{y,center}^{point}$ (for $h$(B/D)) were obtained from the data shown in Fig. 7. The determined values of the correction functions are shown in Fig. 10, where the values of $G$(B/D) and $g$(B/D) are negative because positive $\sigma_x$ at the center of the specimen becomes negative at the end of the specimen (See Fig. 5).

The solid curves in Fig. 10 result from fitting of the data points using the linear combination of exponential functions:

$$M(z) = B_0 + B_1\exp(-w/t_1) + B_2\exp(-w/t_2) \quad (36)$$

where $M$ is the fitting function (for the correction functions $G$, $g$, $H$, $h$, $J$, $j$, $K$ and $k$), $w$ is B/D, and $B_0$, $B_1$, $B_2$, $t_1$ and $t_2$ are the fitting constants shown in Table 2.

At a given load $P$, the developed $\sigma_x$ (compressive) at the loading portion of the flattened specimen ($\sigma_{x,end}^{flattened}$) can be found using $G$(B/D) and $g$(B/D):

$$\sigma_{x,end}^{flattened} = G(B/D)\sigma_{x,center}^{arc} = G(B/D)\frac{2P}{\pi tD\alpha}[\sin 2\alpha - \alpha] \quad (37)$$

$$\sigma_{x,end}^{flattened} = g(B/D)\sigma_{x,center}^{point} = g(B/D)\frac{2P}{\pi tD} \quad (38)$$

The developed $\sigma_y$ (compressive) at the loading portion of the flattened specimen ($\sigma_{y,end}^{flattened}$) at a given load $P$ can also be found using $H$(B/D) and $h$(B/D):

$$\sigma_{y,end}^{flattened} = H(B/D)\sigma_{y,center}^{arc} = -H(B/D)\frac{2P}{\pi tD\alpha}[\sin 2\alpha + \alpha] \quad (39)$$

$$\sigma_{y,end}^{flattened} = h(B/D)\sigma_{y,center}^{point} = -h(B/D)\frac{6P}{\pi tD} \quad (40)$$

The correction functions in Fig. 10 assist the selection of the appropriate value of B/D (the degree of truncation) of the flattened specimen in order to avoid an excessively high development of compressive stresses ($\sigma_x$ and $\sigma_y$) at the loading portion.

### 4.5 Correction functions at a point of interest

As mentioned in Fig. 7(a), in the loading axis of the flattened specimen, the magnitude of $\sigma_y$ is maximum at some distance away from the end (loading portion) of the specimen. When we utilize the flattened specimen in the diametral test, the knowledge of the stress components ($\sigma_{x,max}^{flattened}$ and $\sigma_{y,max}^{flattened}$) at such a location may be of interest. Here we provide the correction functions that are used to determine $\sigma_{x,max}^{flattened}$ and $\sigma_{y,max}^{flattened}$. The ratios of $\sigma_{x,max}^{flattened}/\sigma_{x,center}^{arc}$ (for $J$(B/D)) and $\sigma_{x,max}^{flattened}/\sigma_{x,center}^{point}$ (for $j$(B/D)) were obtained from the data shown in Fig. 6. The ratios of $\sigma_{y,max}^{flattened}/\sigma_{y,center}^{arc}$ (for $K$(B/D)) and

Table 2 Parameters for the fitting function $M$ (Eq. (36)) in the $w$ (=B/D) range of $0.05 \le w \le 0.5$

| Correction functions | $B_0$ | $B_1$ | $t_1$ | $B_2$ | $t_2$ | $R^2$ |
|---|---|---|---|---|---|---|
| $G$ | -0.74795 | -11.9316 | 0.15688 | -41.23803 | 0.03627 | 0.99999 |
| $g$ | -0.21303 | -41.37823 | 0.03678 | -12.01577 | 0.16698 | 0.99998 |
| $H$ | 0.76023 | 4.64947 | 0.13049 | 17.61796 | 0.03093 | 1.00000 |
| $h$ | 0.61878 | 17.41398 | 0.03258 | 4.27830 | 0.14751 | 0.99999 |
| $J$ | 10.17196 | -15.30313 | 0.06521 | -12.53952 | 2.03073 | 0.99993 |
| $j$ | 1.09908 | -14.33099 | 0.06080 | -4.67106 | 0.29529 | 0.99998 |
| $K$ | 0.85510 | 22.53439 | 0.02817 | 5.15135 | 0.12475 | 1.00000 |
| $k$ | 0.70270 | 21.81991 | 0.02999 | 4.68531 | 0.14195 | 0.99999 |

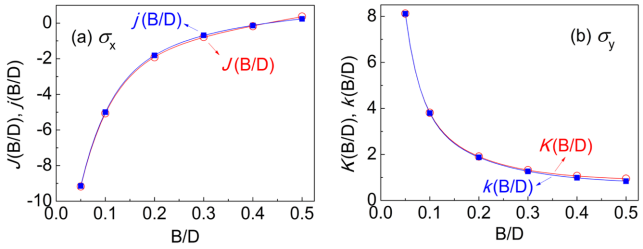


Fig. 11 Correction functions to determine (a) $\sigma_x$ and (b) $\sigma_y$ at the point with maximum magnitude of $\sigma_y$ in the loading axis of the flattened specimen

$\sigma_{y,max}^{flattened} / \sigma_{y,center}^{point}$ (for $k$(B/D)) were obtained from the data shown in Fig. 7. The determined values of the correction functions are shown in Fig. 11. The solid curves in Fig. 11 result from fitting of the data points using Eq. (36) and the fitting constants are shown in Table 2. At a given load $P$, these correction functions allow the determination of $\sigma_{x,max}^{flattened}$ and $\sigma_{y,max}^{flattened}$:

$$\sigma_{x,max}^{flattened} = J(B/D)\,\sigma_{x,center}^{arc} = J(B/D)\frac{2P}{\pi tD\alpha}[\sin 2\alpha - \alpha] \quad (41)$$

$$\sigma_{x,max}^{flattened} = j(B/D)\,\sigma_{x,center}^{point} = j(B/D)\frac{2P}{\pi tD} \quad (42)$$

$$\sigma_{y,max}^{flattened} = K(B/D)\,\sigma_{y,center}^{arc} = -K(B/D)\frac{2P}{\pi tD\alpha}[\sin 2\alpha + \alpha] \quad (43)$$

$$\sigma_{y,max}^{flattened} = k(B/D)\,\sigma_{y,center}^{point} = -k(B/D)\frac{6P}{\pi tD} \quad (44)$$

### 4.6 Overall discussion

In diametral testing, it should not be overlooked that the determined tensile strength receives a full credit only when the specimen is sufficiently resistant to the compressive stress and fails solely because the tensile stress reaches the maximally tolerable value in the axis of loading ($y$-axis). However, even for brittle materials such as ceramics, there is no guarantee that the specimen will fail when the tensile *stress* reaches the maximally tolerable value. For instance, the strength values obtained in diametral testing are generally much lower than the values determined by flexural testing where a purely tensile stress is loaded at the fracturing side of the flexural specimen. According to Wright,[32] such a phenomenon is explained by assuming that the brittle specimen fails when the maximally tolerable *strain* is reached because, in the diametral test, the center of the specimen is also subjected to a compressive stress perpendicular to the tensile stress, and the strains produced by the two stresses are in the same direction.

Table 3 Application of correction function $e$(B/D) to the test results of Fahad[28]

| Dimension | D=40 mm, t=10 mm | | | D=50 mm, t=10 mm | |
|---|---|---|---|---|---|
| B/D | 0 | 0.2 | 0.3 | 0 | 0.2 |
| $\sigma_f^{point}$ (MPa) | 3.38 | 4.76 | 6.16 | 3.47 | 4.14 |
| $e$(B/D) | 1 | 0.91631 | 0.81647 | 1 | 0.91631 |
| $\sigma_f^{flattened}$(MPa) | 3.38 | 4.362 | 5.029 | 3.47 | 3.794 |

Therefore, even though the specimen avoids the fracture at the loading area and the fracture takes place along the loading axis ($y$-axis) by the tensile stress ($\sigma_x$), the fracture of the diametral test should not be regarded as a phenomenon that takes place under a purely tensile mode, because, as mentioned, the diametral specimen fails at the center of the specimen under the presence of not only the tensile stress but also the compressive stress. Only with knowledge of the magnitude of the developed compressive stress as well as the tensile stress within the flattened specimen can physical meanings be assigned to the result of the diametral testing. In this regard, the correction functions provided here may be useful for the analysis of the stress state of a flattened specimen with an arbitrary degree of truncation. They are also the tools for the design of the flattened specimen with an appropriate B/D value from the viewpoint of avoiding an excessively high compressive stress at the loading portion without much sacrifice of the tensile stress at the center of the specimen.

As an example of utilizing the correction functions to obtain stress information of the flattened specimen, the fracture strengths of the flattened specimens reported in Fahad[28] were corrected in this study using correction function $e$(B/D). Table 3 shows the corrected tensile strength of the flattened specimen. In this table, $\sigma_f^{point}$ is the measured tensile strength of the flattened specimen by Fahad[28] based on the Hertz solution (Eq. (8)). $\sigma_f^{flattened}$ is the corrected tensile strength of the flattened specimen using correction function $e$(B/D): $\sigma_f^{flattened} = e(B/D)\,\sigma_f^{point}$. In Table 3, before the correction, the tensile strengths of the flattened specimen based on the Hertz solution ($\sigma_f^{point}$) show a fairly high degree of data scatter: 4.767±1.390 MPa and 3.805±0.474 MPa for the specimens with $D$=40 mm and $D$=50 mm, respectively. However, the corrected tensile strengths of the flattened specimens ($\sigma_f^{flattened}$) show more uniform values: 4.257±0.829 MPa and 3.632±0.229 MPa. This is because the measured tensile strength data of the flattened specimen ($\sigma_f^{point}$) decreases by the correction function $e$(B/D) according

to the degree of truncation of the specimen (the B/D value).

## 5. Conclusions

The stress components at three important locations of the flattened specimen (with varying degrees of truncation, $w$) were obtained numerically by finite element analysis. The obtained stresses ($\sigma_x$ and $\sigma_y$) at each location were compared with the analytical solutions (Hondros solutions) at the center of the arc-loaded specimen with half-arc angle $\alpha$ corresponding to the $w$ value of the flattened specimen. They were also compared with the analytical solutions (Hertz solutions) at the center of the point-loaded specimen without regard to the $w$ value of the flattened specimen. The correction functions were provided as a function of $w$. The stress state of the flattened specimen with an arbitrary degree of truncation can be analyzed using the correction functions. The design of the flattened disk specimen with an appropriate value of $w$ (the degree of the truncation) is also possible using the correction functions from the viewpoint of avoiding an excessively high compressive stress at the loading portion without much sacrifice of the tensile stress at the center of the specimen.

## ACKNOWLEDGMENT

This study was financially supported by the Foundation Research Program under contract No. UD140050GD through an Agency for Defense Development grant funded by the DAPA.

## REFERENCES

1. Carneiro, F. L. L. B. and Barcellos, A., "Concrete Tensile Strength, Union of Testing and Research Laboratories for Materials and Structures," No. 13, 1953.
2. Akazawa, T., "Tension Test Method for Concrete, International Association of Testing and Research Laboratories for Materials and Structures," Bulletin, No. 16, 1953.
3. Frocht, M. M., "Photoelasticity," John Wiley, pp. 121-131, 1948.
4. Hertz, H., "Gesammelte Werke (Collected Works)," Leipzig, pp. 179-185, 1895.
5. Swab, J. J., Yu, J., Gamble, R., and Kilczewski, S., "Analysis of the Diametral Compression Method for Determining the Tensile Strength of Transparent Magnesium Aluminate Spinel," International Journal of Fracture, Vol. 172, No. 2, pp. 187-192, 2011.
6. Sivakugan, N., Das, B. M., Lovisa, J., and Patra, C. R., "Determination of c and $\pi$ of Rocks from Indirect Tensile Strength and Uniaxial Compression Tests," International Journal of Geotechnical Engineering, Vol. 8, No. 1, pp. 59-65, 2014.
7. Martin, E., Pavia, F., Ventrella, A., Avalle, M., Lara-Curzio, E., and Ferraris, M., "A Brazilian Disk Test for the Evaluation of the Shear Strength of Epoxy-Joined Ceramics," International Journal of Applied Ceramic Technology, Vol. 9, No. 4, pp. 808-815, 2012.
8. Kim, J.-D., Lee, S.-J., and Suh, J., "Microstructural Variations and Machining Characteristics of Silicon Nitride Ceramics from Increasing the Temperature in Laser Assisted Machining," Int. J. Precis. Eng. Manuf., Vol. 15, No. 7, pp. 1269-1274, 2014.
9. Wang, J.-C., "A Novel Fabrication Method of High Strength Alumina Ceramic Parts Based on Solvent-Based Slurry Stereolithography and Sintering," Int. J. Precis. Eng. Manuf., Vol. 14, No. 3, pp 485-491, 2013.
10. Choi, W. and Kim, J., "Fractal Dimensional Analysis on Glass Fracture," Int. J. Precis. Eng. Manuf., Vol. 16, No. 7, pp. 1655-1669, 2015.
11. Choi, Y.-J., Song, M.-S., Yoo, Y.-J., and Lee, J.-S., "Fracture Analysis for Ceramic Disk with Semi-Elliptical Crack and Pore," Int. J. Precis. Eng. Manuf., Vol. 15, No. 3, pp. 433-438, 2014.
12. Xiao, Y., Chen, M.-J., Yang, Y.-T., and Chen, J., "Research on the Critical Condition of Brittle-Ductile Transition about Micro-Milling of KDP Crystal and Experimental Verification," Int. J. Precis. Eng. Manuf., Vol. 16, No. 2, pp. 351-359, 2015.
13. Hondros, G., "The Evaluation of Poisson's Ratio and the Modulus of Materials of a Low Tensile Resistance by the Brazilian (Indirect Tensile) Test with Particular Reference to Concrete," Australian Journal of Applied Science, Vol. 10, No. 3, pp. 243-268, 1959.
14. Rodríguez, J., Navarro, C., and Sánchez-Gálvez, V., "Splitting Tests: An Alternative to Determine the Dynamic Tensile Strength of Ceramic Materials," Journal de Physique IV, Vol. 4, No. C8, pp. C8-101-C108-106, 1994.
15. Dai, F., Xia, K., and Luo, S., "Semicircular Bend Testing with Split Hopkinson Pressure Bar for Measuring Dynamic Tensile Strength of Brittle Solids," Review of Scientific Instruments, Vol. 79, No. 12, Paper No. 123903, 2008.
16. Dong, S., Wang, Y., and Xia, Y., "A Finite Element Analysis for using Brazilian Disk in Split Hopkinson Pressure Bar to Investigate Dynamic Fracture Behavior of Brittle Polymer Materials," Polymer Testing, Vol. 25, No. 7, pp. 943-952, 2006.
17. Zhou, Y., Xia, K., Li, X., Li, H., Ma, G., et al., "Suggested Methods For Determining the Dynamic Strength Parameters and Mode-I Fracture Toughness of Rock Materials," International Journal of Rock Mechanics and Mining Sciences, Vol. 49, pp. 105-112, 2012.
18. Zhang, Q. B. and Zhao, J., "Determination of Mechanical Properties and Full-Field Strain Measurements of Rock Material under Dynamic Loads," International Journal of Rock Mechanics and Mining Sciences, Vol. 60, pp. 423-439, 2013.
19. Zhang, Q. B. and Zhao, J., "A Review of Dynamic Experimental Techniques and Mechanical Behaviour of Rock Materials," Rock Mechanics and Rock Engineering, Vol. 47, No. 4, pp. 1411-1478, 2014.
20. Pramanik, B., Mantena, P. R., Tadepalli, T., and Rajendran, A. M.,

"Indirect Tensile Characterization of Graphite Platelet Reinforced Vinyl Ester Nanocomposites at High-Strain Rate," Open Journal of Composite Materials, Vol. 4, No. 4, pp. 201-214, 2014.

21. Xia, K. and Yao, W., "Dynamic Rock Tests using Split Hopkinson (Kolsky) Bar System-A Review," Journal of Rock Mechanics and Geotechnical Engineering, Vol. 7, No. 1, pp. 27-59, 2015.
22. Grantham, S. G., Siviour, C. R., Proud, W. G., and Field, J. E., "High-Strain Rate Brazilian Testing of an Explosive Simulant using Speckle Metrology," Measurement Science and Technology, Vol. 15, No. 9, pp. 1867-1870, 2004.
23. Siviour, C. R., Grantham, S. G., Williamson, D. M., Proud, W. G., and Field, J. E., "Novel Measurements of Material Properties at High Rates of Strain using Speckle Metrology," The Imaging Science Journal, Vol. 57, No. 6, pp. 326-332, 2009.
24. Siviour, C. R., Laity, P. R., Proud, W. G., Field, J., Porter, D., et al., "High Strain Rate Properties of a Polymer-Bonded Sugar: Their Dependence on Applied and Internal Constraints, Proceedings of the Royal Society of London A: Mathematical," Physical and Engineering Sciences, Vol. 464, No. 2093, pp. 1229-1255, 2008.
25. Wang, Q., Li, W., and Xie, H., "Dynamic Split Tensile Test of Flattened Brazilian Disc of Rock with SHPB Setup," Mechanics of Materials, Vol. 41, No. 3, pp. 252-260, 2009.
26. Wang, Q.-Z. and Xing, L., "Determination of Fracture Toughness KIC by using the Flattened Brazilian Disk Specimen for Rocks," Engineering Fracture Mechanics, Vol. 64, No. 2, pp. 193-201, 1999.
27. Wang, Q. Z., Jia, X. M., Kou, S. Q., Zhang, Z. X., and Lindqvist, P.-A., "The Flattened Brazilian Disc Specimen Used for Testing Elastic Modulus, Tensile Strength and Fracture Toughness of Brittle Rocks: Analytical and Numerical Results," International Journal of Rock Mechanics and Mining Sciences, Vol. 41, No. 2, pp. 245-253, 2004.
28. Fahad, M. K., "Stresses and Failure in the Diametral Compression Test," Journal of Materials Science, Vol. 31, No. 14, pp. 3723-3729, 1996.
29. Es-Saheb, M. H., Albedah, A., and Benyahia, F., "Diametral Compression Test: Validation using Finite Element Analysis," The International Journal of Advanced Manufacturing Technology, Vol. 57, No. 5-8, pp. 501-509, 2011.
30. Yoo, Y.-H., Lee, W., and Shin, H., "Spherical Nano-Indentation of a Hard Thin Film/Soft Substrate Layered System: I. Critical Indentation Depth," Modelling and Simulation in Materials Science and Engineering, Vol. 12, No. 1, pp. 59-67, 2004.
31. Yoo, Y.-H., Lee, W., and Shin, H., "Spherical Nano-Indentation of a Hard Thin Film/Soft Substrate Layered System: II. Evolution of Stress and Strain Fields," Modelling and Simulation in Materials Science and Engineering, Vol. 12, No. 1, pp. 69-78, 2004.
32. Wright, P. J. F., "Comments on an Indirect Tensile Test on Concrete Cylinders," Magazine of Concrete Research, Vol. 7, No. 20, pp. 87-96, 1955.